General Disclaimer

One or more of the Following Statements may affect this Document

- This document has been reproduced from the best copy furnished by the organizational source. It is being released in the interest of making available as much information as possible.

- This document may contain data, which exceeds the sheet parameters. It was furnished in this condition by the organizational source and is the best copy available.

- This document may contain tone-on-tone or color graphs, charts and/or pictures, which have been reproduced in black and white.

- This document is paginated as submitted by the original source.

- Portions of this document are not fully legible due to the historical nature of some of the material. However, it is the best reproduction available from the original submission.

X-932-75-168
PREPRINT

NASA TM X- 71016

RECOVERY OF ATMOSPHERIC REFRACTIVITY PROFILES FROM SIMULATED SATELLITE-TO-SATELLITE TRACKING DATA

C. W. MURRAY, JR.
S. RANGASWAMY

JUNE 1975

GSFC

GODDARD SPACE FLIGHT CENTER
GREENBELT, MARYLAND

RECOVERY OF ATMOSPHERIC REFRACTIVITY PROFILES FROM SIMULATED SATELLITE-TO-SATELLITE TRACKING DATA

C. W. Murray, Jr.
S. Rangaswamy

ABSTRACT

Two techniques for recovering atmospheric refractivity profiles from simulated satellite-to-satellite tracking data are documented and the relative degradation in accuracy due to the calculation methods shown (modelling errors not included). Examples are given using the geometric configuration of the ATS-6/NIMBUS-6 Tracking Experiment. Both satellites are in circular orbit (NIMBUS in polar orbit at a height of 1000 kilometers and ATS in a geostationary equatorial orbit). The underlying refractivity model for the lower atmosphere has the spherically symmetric form $N = \exp P(s)$ where $P(s)$ is a polynomial in the normalized height s. For the particular simulation used in the analysis, the Herglotz-Wiechert technique recovered values which were 0.4% and 40% different from the input values (calculated from the parameters of the assumed model atmosphere) at the surface and at a height of 33 kilometers, respectively. Using the same input data, the model fitting technique recovered refractivity values 0.05% and 1% different from the input values at the surface and at a height of 50 kilometers, respectively.

It is also shown that if ionospheric and water vapor effects can be properly modelled or effectively removed from the data (e.g., by separate measurement such as a radiometer or by regression techniques), pressure and temperature distributions can be obtained from the dry refractivity by numerical integration, assuming hydrostatic equilibrium and the perfect gas law. This is demonstrated for radiosonde data taken at Dulles airport, where pressure is recovered to less than 0.3% up to 20 kilometers. The temperature recovery for the particular example was 5% at the surface but improved with height.

CONTENTS

ILLUSTRATIONS

TABLES

RECOVERY OF ATMOSPHERIC REFRACTIVITY PROFILES FROM SIMULATED SATELLITE-TO-SATELLITE TRACKING DATA

1.0 INTRODUCTION

The purpose of this report is two-fold: (1) to document two techniques for recovering lower atmospheric refractivity profiles[1] from simulated satellite-to-satellite tracking data, and; (2) to show how pressure and temperature can be calculated from the recovered refractivity profile provided the effects of the ionosphere and water vapor are properly modelled or effectively removed from the data. Also shown are the effects of the atmosphere upon the one-way range and range rate between the two satellites.

Both the geometry of satellite-to-satellite tracking and precise range and range rate measurements expected in the ATS-6/NIMBUS-6 Tracking and Orbit Determination Experiment [1] have provided the motivation for the present analysis.

The geometry used for the simulation can be seen in Figure 1 where NIMBUS is in a circular polar orbit of 1000 kilometers and ATS is in a geostationary orbit in the equatorial plane.[2]

The tracking signal travels a 4-way path: from the ground station to ATS, from ATS to NIMBUS, from NIMBUS to ATS, and ATS back to ground.

Radio occultation occurs whenever the signal between the two satellites passes through the atmosphere. As NIMBUS emerges from or enters into radio shadow behind the earth, the phase of the tracking signal between the two satellites is affected by the presence of the earth's atmosphere. Given the ephemeris of each satellite and the tracking data (range and/or range rate), it is possible to obtain a vertical refractivity profile of the earth's lower atmosphere above the point where the ray path between the satellites comes closest to the earth.

[1] For this analysis the lower atmosphere is defined to be the neutral atmosphere from the surface of the earth to an altitude of 100 kilometers. The ionosphere is defined as that part of the atmosphere containing charged particles in sufficient density to affect the propagation of S-band signals (2 GHz) and extending from an altitude of 100 kilometers to 1000 kilometers.

[2] NIMBUS-6 was successfully launched 12 June 1975 and is in a near-circular orbit (eccentricity of $\sim$0.0008) at an altitude of 1000 kilometers and inclination of approximately 100°. ATS-6 is also in a near-circular orbit (eccentricity of $\sim$0.0003) with an inclination of 0.9° and semi-major axis of about 41870 kilometers. The orbits of ATS and NIMBUS are assumed to be circular for simplicity in analysis.

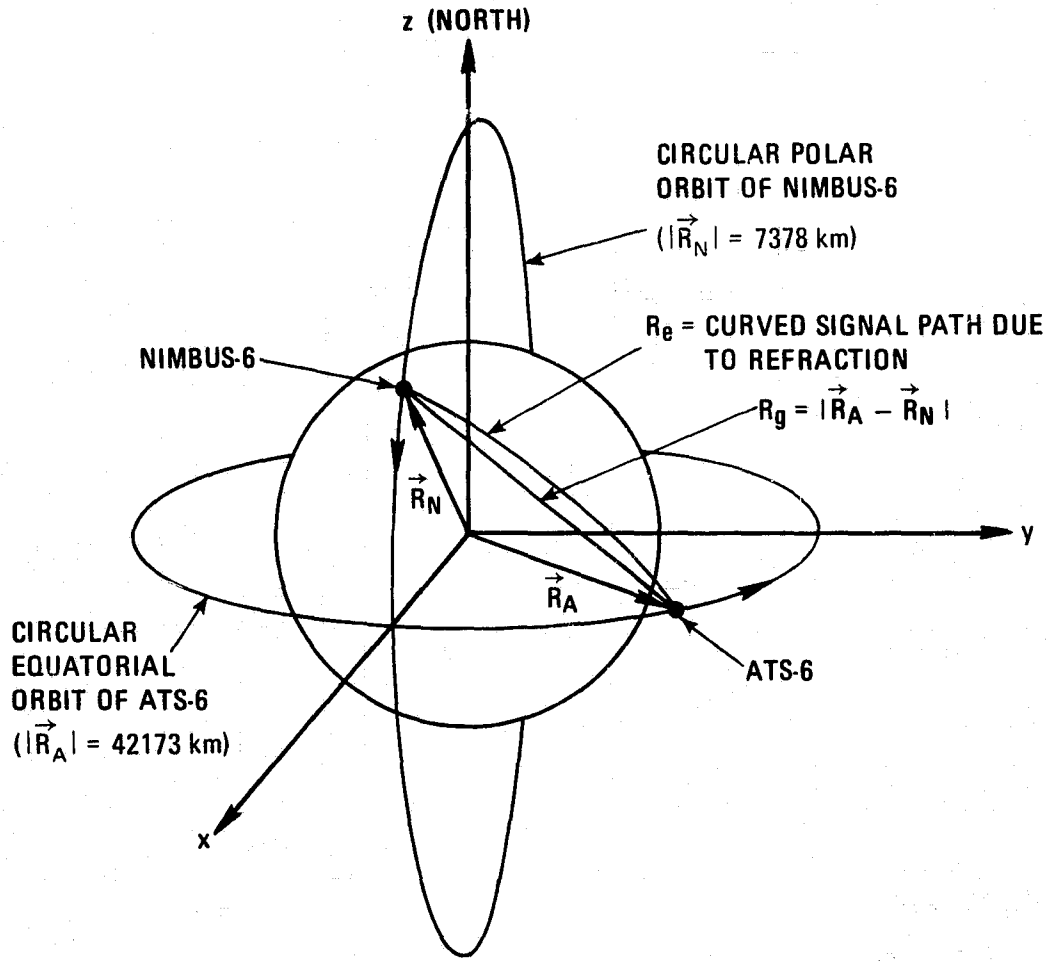

NOTE: FIGURE DOES NOT DEPICT NOMINAL OR ACTUAL ORBITS.
CIRCULAR ORBITS ASSUMED

Figure 1. ATS-6/NIMBUS-6 Geometry

The mathematical techniques of profile inversion are well-documented [2] and planetary atmospheres have been studied using microwave radio occultation methods for Mars ([3], [4], [5]) and Venus ([6], [7], [8]). In [9] it is pointed out that the ATS-6/NIMBUS-6 Tracking Experiment provides a ready-made opportunity for measuring atmospheric profiles of the earth. Marini [9] assumes an exponential model for the lower atmosphere and a parabolic model for the ionospheric density and gives the errors in range and range rate between the two satellites for a 2 GHz carrier signal. The calculations are made for straight line propagation and show measurable atmospheric effects of 150 meters in range

and 50 meters/second in range rate and ionospheric effects of 15 meters in range and 30 centimeters/second in range rate.

Both the Herglotz-Wiechert method and the iterative model-fitting approach which are described in this analysis can be found in the literature [2]. They have been adapted for use here in order to meet the geometrical constraints imposed by the ATS-6/NIMBUS-6 Tracking and Orbit Determination Experiment [1].

2.0 TRACKING MEASUREMENTS

For the ATS-6/NIMBUS-6 Tracking Experiment [1], the signal travels a 4-way path as shown in Figure 2 which is taken from [1]. The range measurement consists of the time in seconds between a zero crossing of the ground transmitted signal (6 GHz carrier phase modulated by a 100 KHz sidetone) and a zero

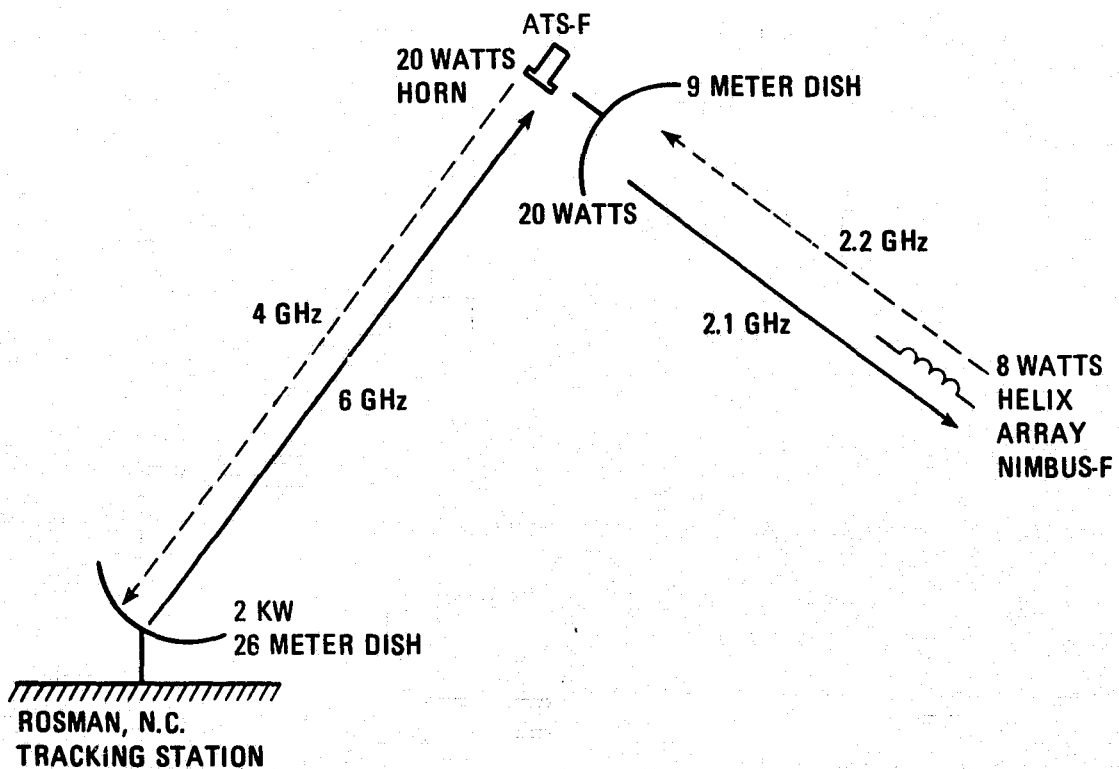

Figure 2. Tracking Measurements (taken from [1])

crossing of the ground received signal (4 GHz carrier having two subcarriers each phase modulated by the 100 KHz sidetone) after the signal has travelled from ground to ATS, to NIMBUS, back to ATS, and then to ground ([10]). The range rate measurement consists of the time in seconds required to count a fixed number of cycles of the 4-way Doppler frequency plus a fixed offset frequency. (Destruct Mode, [10].)

For purposes of this report the "observables" are the one-way range between NIMBUS (at the time the signal leaves there) and ATS (at the time the signal arrives there) along the propagation path of the signal and the rate of change of this quantity with time or range rate along the propagation path.

3.0 LOWER ATMOSPHERIC REFRACTIVITY PROFILE AND MODEL

Refractivity at radio frequencies is given by ([11], pg. 7)

$$N = 77.6\,(P/T) + (3.73)\,10^5\,(e/T^2) \tag{3.1}$$

where P is pressure in millibars, T is temperature in degrees Kelvin, and e is the partial pressure of the water vapor in millibars given by ([12], pg. 343)

$$e = (R_h/100)\,(6.11)\,10^{\frac{7.5\,(T\,-\,273.15)}{237.3\,+\,(T\,-\,273.15)}} \tag{3.2}$$

where R_h is the relative humidity in percent.[3]

Refractivity N is related to the index of refraction n[4] by the following

$$N = (n - 1)\,10^6 \tag{3.3}$$

The first term on the right-hand side of (3.1) is the dry refractivity N_d and the second term on the right-hand side the wet refractivity N_w.

[3]If the dewpoint temperature T_d (°K) is given instead of the relative humidity, e can be calculated from (3.2) by setting R_h equal to 100 and T_d equal to T.

[4]The group and phase index of refraction are the same since the lower atmosphere is assumed to be non-dispersive.

An example of a refractivity profile calculated from tables of pressure, temperature, and relative humidity versus height for a standard atmosphere of 30° North July [13], using (3.1) can be seen in Figure 3. Both the dry and the dry-plus-wet profiles are shown.

It can be seen that $\log_e N$ is almost linear in the height h. Bean and Thayer [14] have found the average variation of N with height to be nearly exponential. Hence, it seems reasonable to model the lower atmospheric refractivity with

$$N = \exp P(s) \tag{3.4}$$

where P(s) is a polynomial in the normalized height $s = (.01)h - 1$ (h is height in kilometers).

Figure 4 shows the residuals from a seventh degree least squares polynomial fit to $\log_e N$ where N is the dry-plus-wet refractivity shown in Figure 3.

Figure 5 shows the increased goodness-of-fit with higher degree polynomial fits to $\log_e N$. Both the dry and the dry-plus-wet refractivities are compared and it is seen that there is little difference between them as the degree is increased.

4.0 EFFECT OF LOWER ATMOSPHERE ON RANGE, RANGE RATE, AND BENDING ANGLE

A radio wave passing through the earth's atmosphere is bent and, in addition, delayed along its path. The first effect is due to the varying index of refraction across the signal path, while the second effect is due to the fact that the index of refraction for the lower atmosphere is greater than unity. Both these effects combine to cause the apparent range between a transmitter and receiver to be greater than the line-of-sight range.

Figure 6 shows the lower atmospheric effects upon range, range rate, and bending angle for a realistic refractivity profile of the form indicated in (3.4) where P(s) is a second degree polynomial. The coefficients of P(s) were determined using linear least squares, fitting the polynomial to the logarithm of the calculated values of refractivity. The refractivity was calculated from radiosonde data taken at Dulles airport, Virginia, in 1967, using (3.1) and the procedure outlined in [15]. The geometric configuration of ATS and NIMBUS is indicated in the figure where ATS is near the orbital plane of NIMBUS.

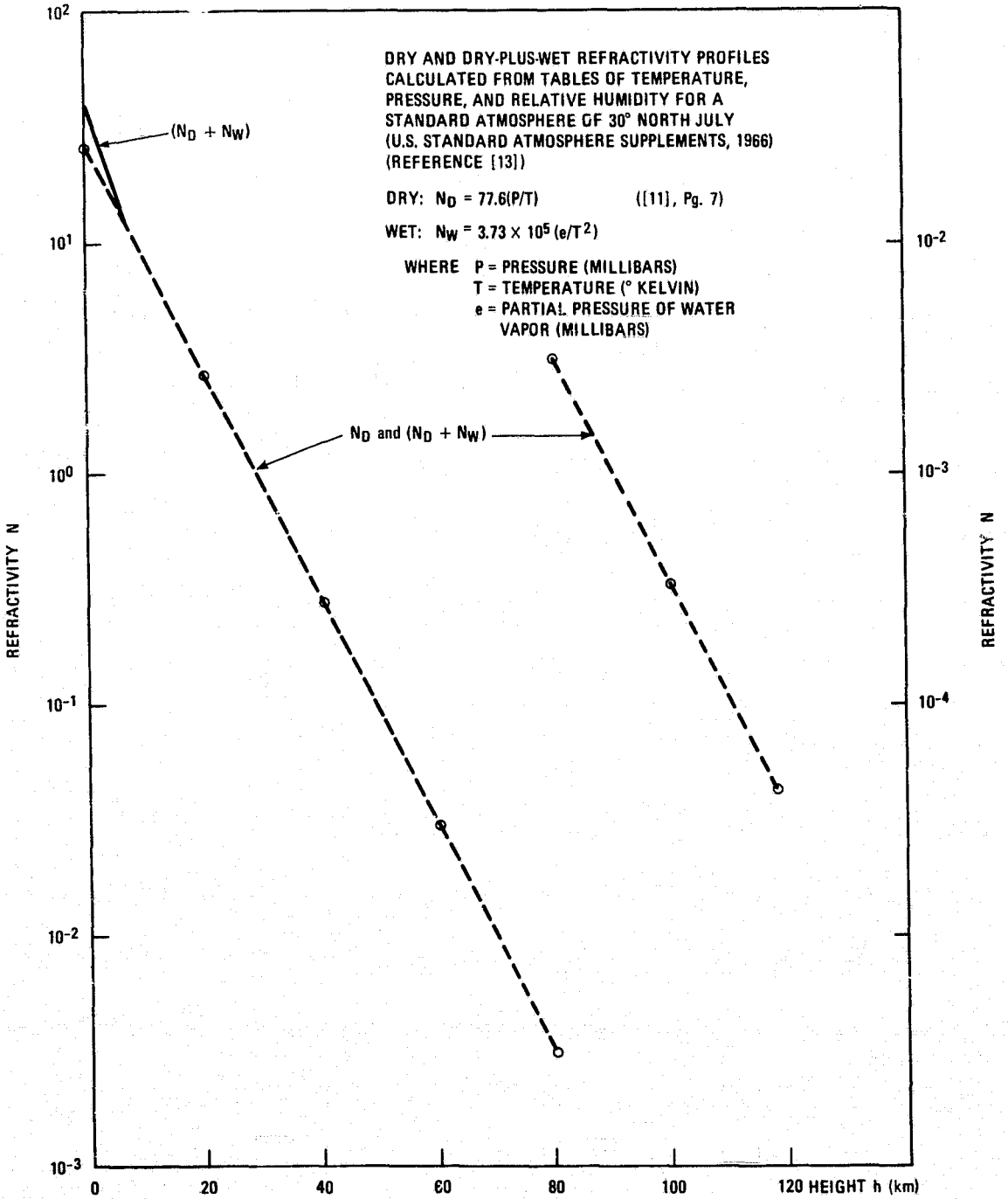

Figure 3. Lower Atmospheric Refractivity Profile

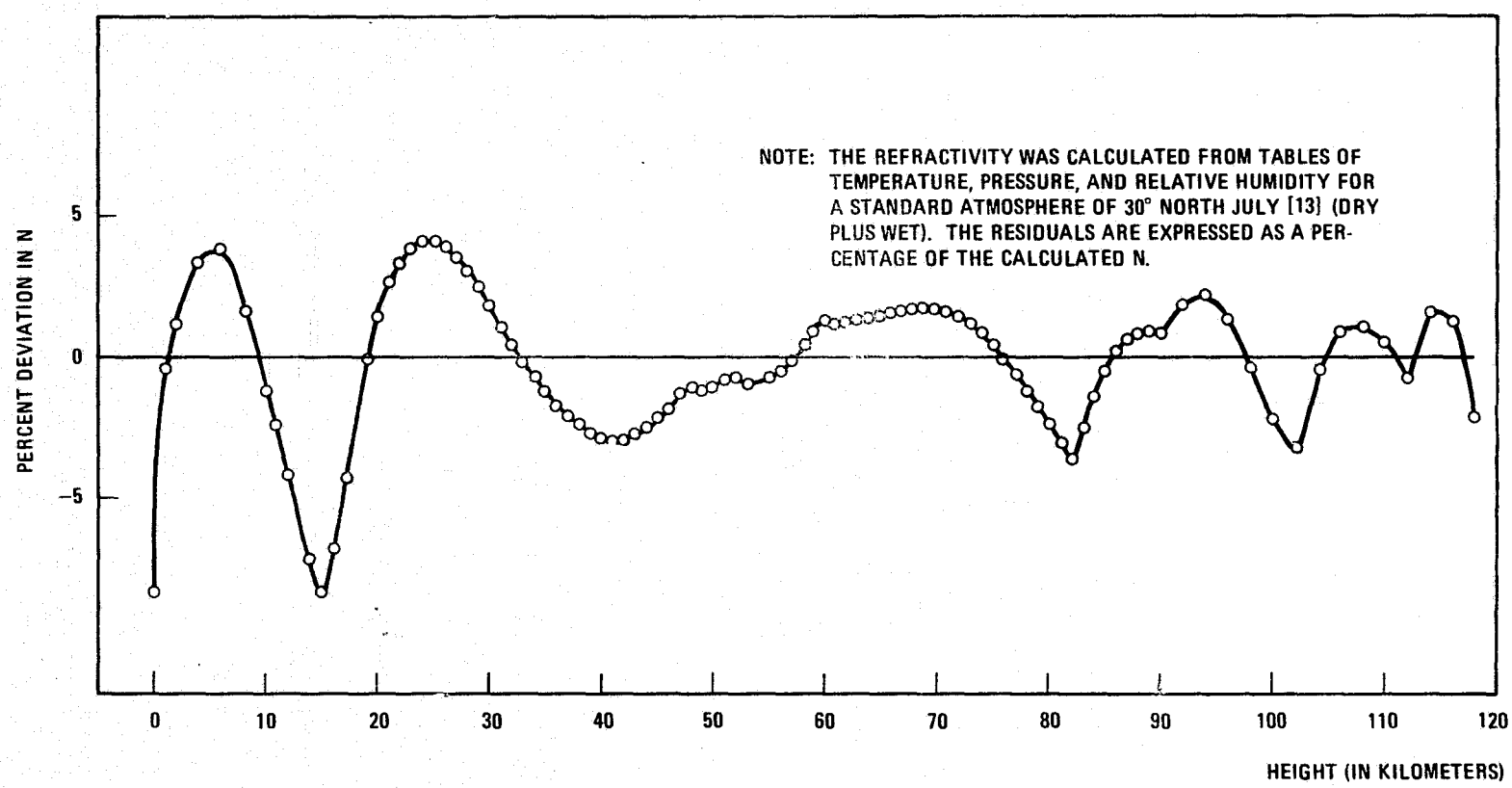

Figure 4. Residuals from a 7th Degree Least Squares Polynomial Fit to the Logarithm of Refractivity

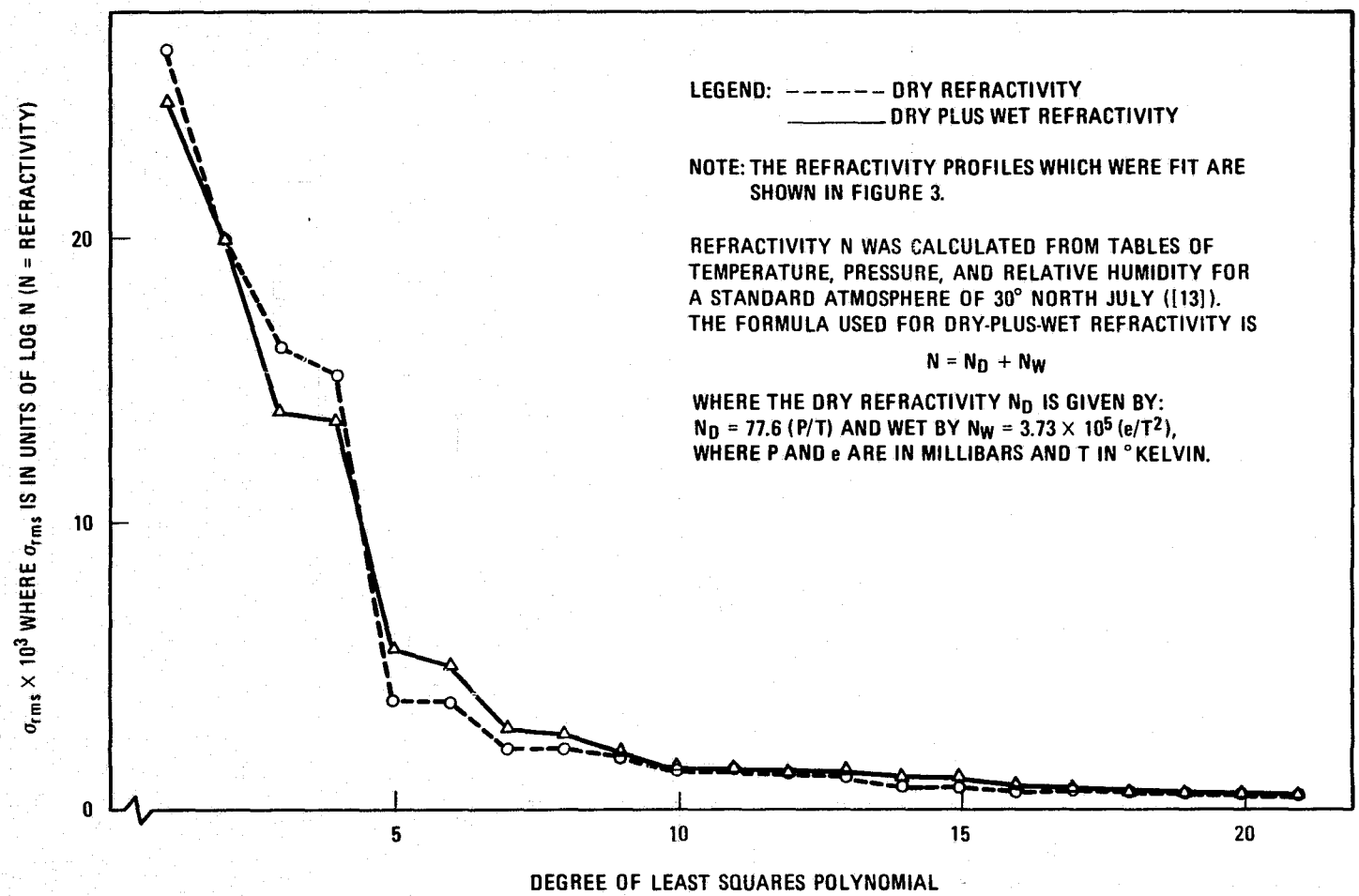

Figure 5. RMS of Least Squares Polynomial Fits to the Logarithm of Refractivity

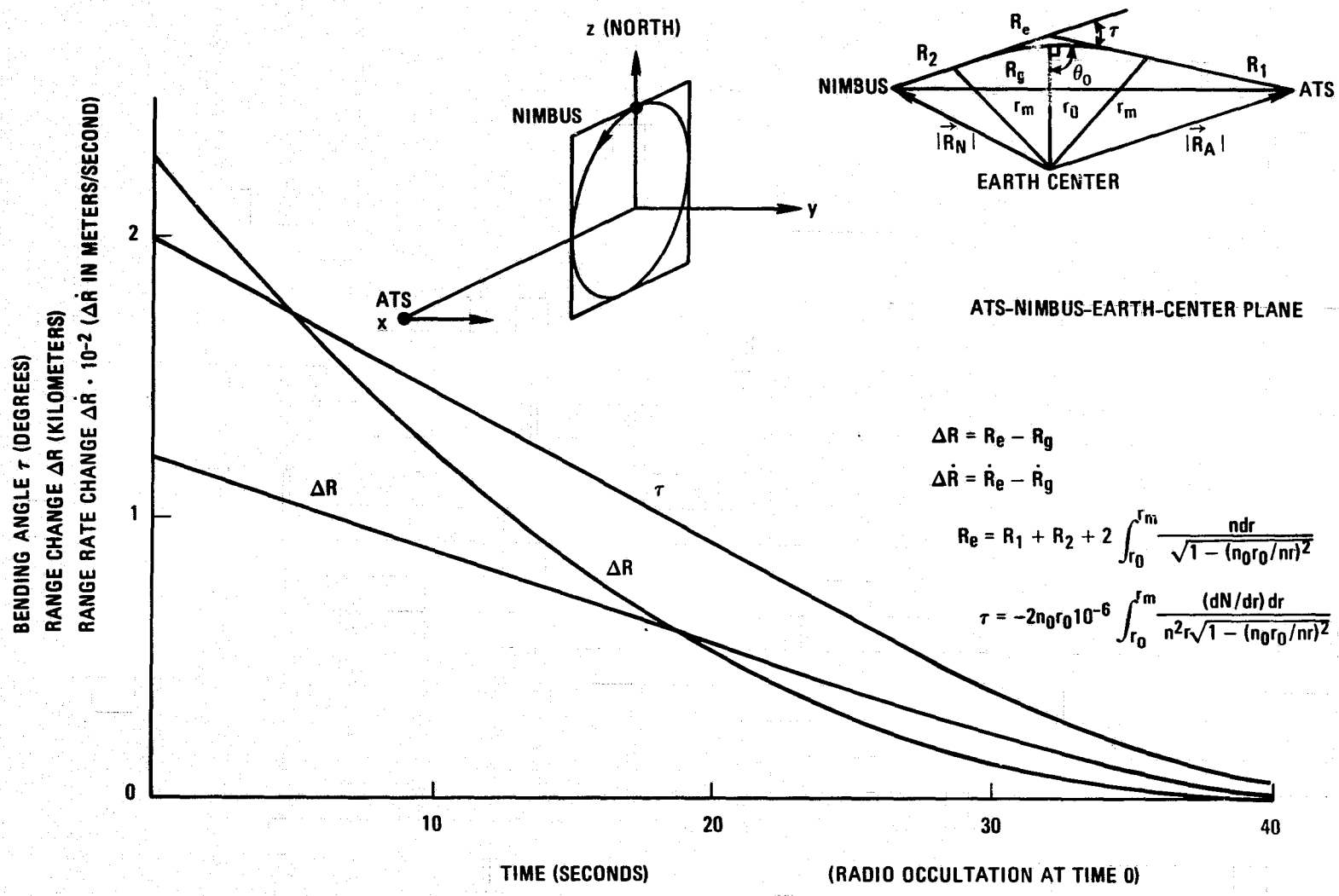

Figure 6. Lower Atmospheric Effects for Typical Refractivity Profile

The range error due to the lower atmosphere (see Figure 6) is

$$\Delta R = R_e - R_g \tag{4.1}$$

where

$$R_e = R_1 + R_2 + 2\int_{r_0}^{r_m} n\,ds$$

or

$$R_e = R_1 + R_2 + 2\int_{r_0}^{r_m} \frac{n\,dr}{\sqrt{1 - (n_0 r_0 / n r)^2}}$$

$$R_g = \vec{R}_N - \vec{R}_A \tag{4.2}$$

and R_1 and R_2 are the linear segments taken from the "top" of the lower atmosphere r_m (at an altitude of 100 kilometers) to the radius of ATS and the radius of NIMBUS, n is the index of refraction at the geocentric radius r, $\vec{R}_A$ and $\vec{R}_N$ are the position vectors of ATS and NIMBUS, R_g is the line-of-sight range.

The bending angle τ [16] is given by

$$\tau_{1,2} = -\int_{n_1}^{n_2} \cot\theta\ (dn/n)$$

or

$$\tau = -2n_0 r_0\, 10^{-6} \int_{r_0}^{r_m} \frac{(dN/dr)\,dr}{n^2 r \sqrt{1 - (n_0 r_0 / n r)^2}} \tag{4.3}$$

using (3.3) and Snell's law for a spherically stratified medium

$$n r \cos \theta = n_0 r_0 \cos \theta_0 \tag{4.4}$$

where θ is the local elevation angle of the ray at radius r and n is the index of refraction at the radius r.

The error in range rate due to the lower atmosphere is

$$\Delta \dot{R} = \dot{R}_e - \dot{R}_g \tag{4.5}$$

where $\dot{R}_e$ is the range rate along the propagation path which is obtained by summing the dot products of the velocity vectors of ATS and NIMBUS with unit vectors along the propagation path at each satellite (using the convention that an increasing range with time gives rise to a positive range rate). The unit vectors are obtained through ray trace procedures and there is a one-to-one correspondence between these vectors and the range $R_e \cdot \dot{R}_g$ is the range rate along the line-of-sight range R_g.

The quantities ΔR, $\Delta \dot{R}$, and τ are obtained as functions of time by linking them to the ephemeris of both satellites.

From the figure the atmospheric range error is more than 2 kilometers and the range rate error more than 100 meters/second at the time of occultation. This is largely due to the bending angle of approximately 2° at the surface.

Figure 7 shows the difference between the atmospheric range error taken along a curved path and the range error taken along a straight line path. Also shown is the difference between these two quantities which is 38 meters at the time of occultation.

The assumption of a straight ray (neglecting bending) simplifies the analysis and is valid for tenuous atmospheres like that of Mars. However, Figures 6 and 7 show that in the case of the earth's atmosphere, refractive bending of the ray cannot be neglected.

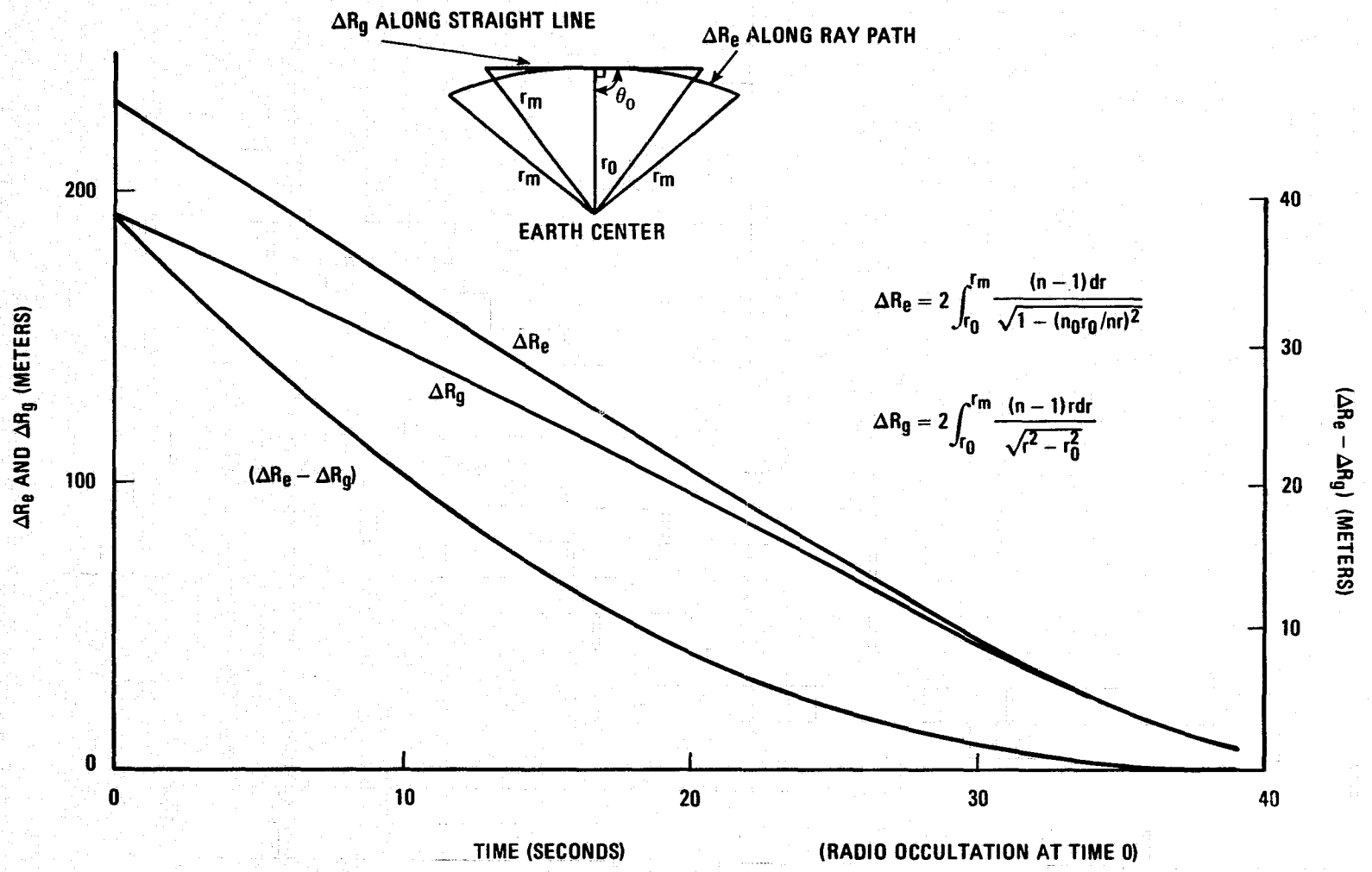

Figure 7. Difference Between Atmospheric Range Error Along a Straight Line and Along the Ray Path of the Signal

5.0 IONOSPHERIC MODEL AND EFFECT OF IONOSPHERE ON TRACKING DATA

Although the main purpose of this analysis is the recovery of lower atmospheric refractivity profiles, the ionosphere cannot be neglected at S-band frequencies (2 GHz). Its effect, however, is not as great as the lower atmosphere upon one-way satellite-to-satellite range and range rate [9]. The manner in which the ionosphere enters into the occultation calculations is in the computation of the path length of the signal through that region (100 to 1000 kilometers). See equation (B.9) of Appendix B. But for rays passing close to the earth, the change in the contribution of the ionosphere to the total path length should be rather small. For this reason and the fact that the ionospheric errors at S-Band are much less than the lower atmospheric errors (in the tracking data), a simple model for the ionospheric density is desirable. The ionosphere is dispersive and therefore the distinction must be made between group and phase velocities and group and phase indices of refraction. The group index of refraction is related to the group refractivity (equation 3.3) by

$$N_g = (n_g - 1)\, 10^6 \tag{5.1}$$

and N_g is given by [17]

$$N_g(h) = \frac{40.3\, N_e(h)}{f^2}\, 10^6 \tag{5.2}$$

where

N_e = electron density (electrons/meter^3)

f = frequency (Hz)

h = height

With the objective of simplicity in mind a Chapman and a modified Chapman function [18] were fit to a composite profile from Alouette-I and Wallops Island ionograms [19].[5] The results can be seen in Figure 8. The modified Chapman function yields a much better fit than the Chapman function up to an altitude of about 700 kilometers.

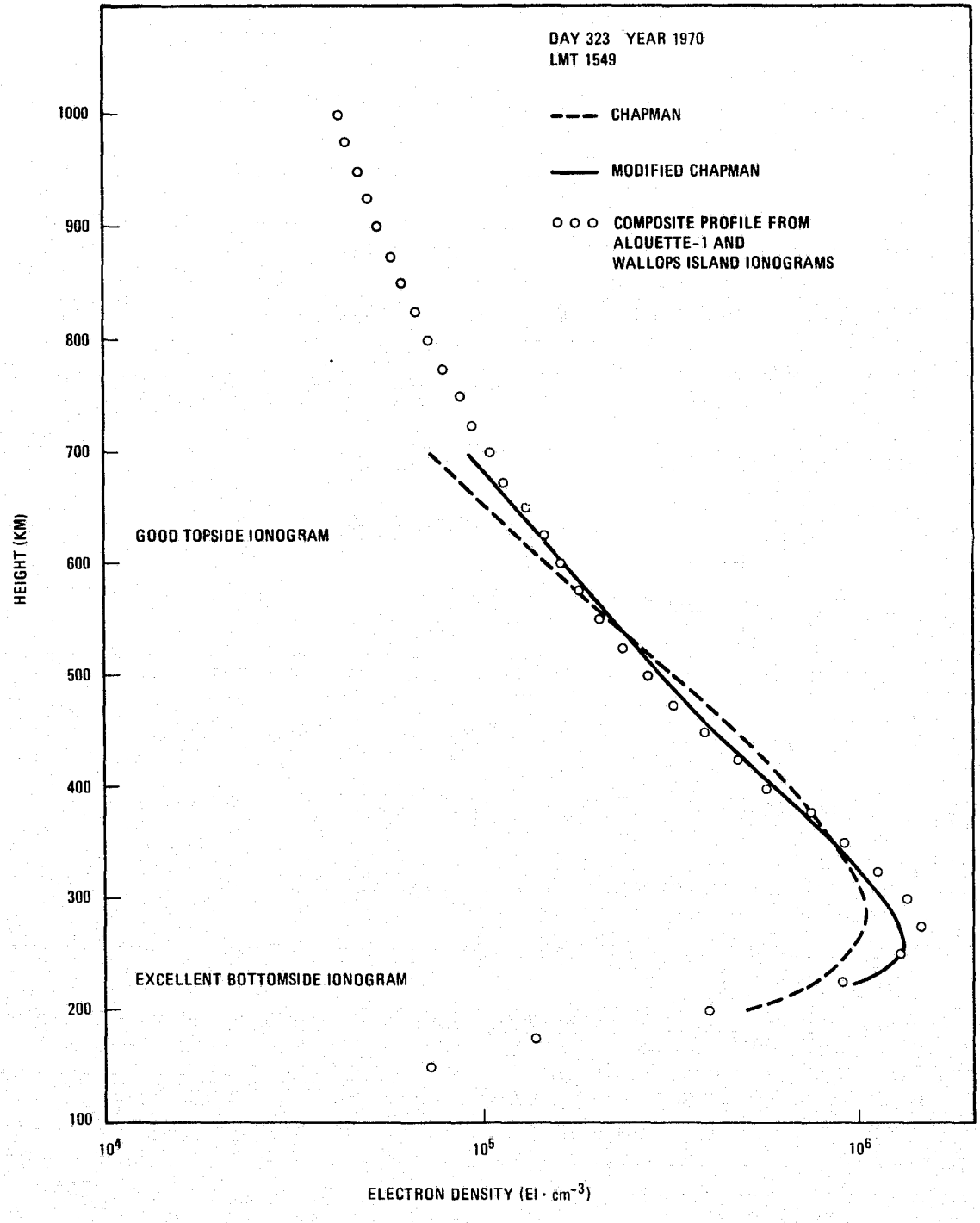

Figure 8. Comparison of Ionospheric Electron Density Models.

Table I shows a comparison of various ionospheric models fit to the composite profile in Figure 8. It can be seen that the exponential polynomial gives the best fit (Columns 3 and 4).

Figure 9 shows the effect of the ionosphere for a typical electron density profile.

The effect of the ionosphere in the recovery of lower atmospheric refractivity profiles is included in the next section.

6.0 ITERATIVE MODEL FITTING TECHNIQUE

The problem here is to determine the parameters of an assumed refractivity model for the lower atmosphere of the form (3.4) given an ephemeris of the two satellites and the one-way range and/or range rate between them for a number of data points. The technique uses the generalized method of nonlinear weighted least squares with apriori parameter vector $\tilde{x}$ and apriori covariance matrix $D_{\tilde{x}}$ (Appendix A) to find the $(m \times 1)$ parameter vector

$$x^T = (a_0\ a_1\ a_2 \ldots a_{m-1}) \tag{6.1}$$

of the polynomial P

$$P = s^T x = a_0 + a_1 s + \ldots + a_{m-1} s^{m-1} \tag{6.2}$$

---

[5]The Chapman profile is given by

$$N(h) = N_{max} \exp \frac{1}{2} (1 - z - e^{-z})$$

where

$N(h)$ = electron density at an altitude h (e/m^3)
N_{max} = maximum electron density (e/m^3)
$z = (h - h_{max})/H$
h_{max} = height at which electron density is maximum
H = scale height

The modified Chapman profile is given by

$$N(h) = N_{max} \exp \frac{1}{2} \left(1 - \frac{z'}{A} - e^{\left(\frac{z'}{A}\right)}\right)$$

$$A = 1 - \exp\left(\frac{-\alpha z'}{2}\right)$$

$$z' = (h - h_{max})/H_0$$

the parameters of the model being N_{max}, h_{max}, α and H_0.

Table I

Comparison of Various Ionospheric Models Fit to Composite Electron Density Profile in Figure 8

DAY 323, 1970 LMT 1549 SOL. ZEN. ANGLE 80.5°

Altitude (km)	Electron Density (10^{12} Electrons/m^3)				
	Composite Profile	Polynomial Degree 7	Polynomial Degree 10	Chapman	Modified Chapman
200	0.41	0.40	0.40	0.50	0.39
250	1.29	1.29	1.30	0.93	1.29
275	1.43	1.46	1.43	1.02	1.29
300	1.34	1.32	1.33	1.02	1.15
325	1.13	1.11	1.12	0.95	0.99
350	0.91	0.90	0.91	0.86	0.84
400	0.58	0.58	0.58	0.65	0.59
450	0.38	0.39	0.39	0.46	0.42
500	0.27	0.27	0.27	0.32	0.30
550	0.21	0.21	0.21	0.22	0.22
600	0.16	0.16	0.16	0.15	0.16
650	0.13	0.13	0.13	0.10	0.12
700	0.10	0.10	0.10	0.07	0.09
750	0.08	0.08	0.08		
800	0.07	0.07	0.07		
850	0.06	0.06	0.06		
900	0.05	0.05	0.05		
950	0.05	0.05	0.05		
1000	0.04	0.04	0.04		

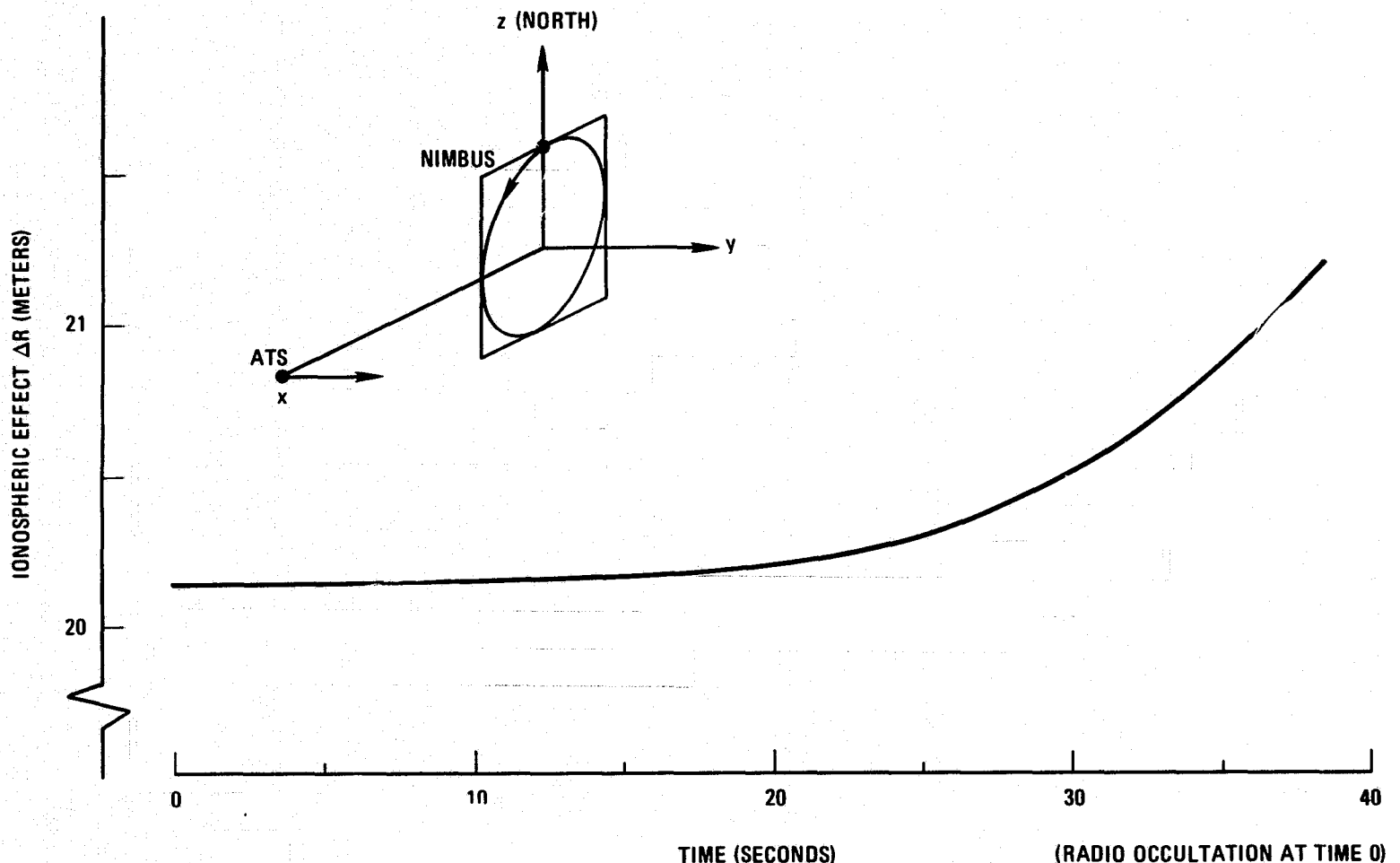

Figure 9. Ionospheric Effect for Typical Ionospheric Density

in the model (3.4)

$$N = \exp P(s) \tag{6.3}$$

which minimizes the quadratic form

$$Q = \left[z - f(x)\right]^T D_z^{-1} \left[z - f(x)\right] + (x - \tilde{x})^T D_{\tilde{x}}^{-1} (x - \tilde{x}) \tag{6.4}$$

The vector s

$$s^T = (1 \; s \; s^2 \; \ldots \; s^{m-1}) \tag{6.5}$$

is the vector of normalized heights $s = (0.01)\,s - 1$ (h is the height in kilometers).

The vector $\tilde{x}$

$$\tilde{x}^T = (\tilde{a}_0 \; \tilde{a}_1 \; \tilde{a}_2 \; \ldots \; \tilde{a}_{m-1}) \tag{6.6}$$

is the apriori vector of assumed starting values for the coefficients a_j in (6.2) with associated covariance matrix $D_{\tilde{x}}$.

The vector z

$$z^T = (z_1 \; z_2 \; \ldots \; z_n) \tag{6.7}$$

is the observation vector (range and/or range rate values) with covariance matrix D_z (taken to be the identity matrix in this report, i.e., least squares with equal weights).

The vector f

$$f^T = (f_1 \; f_2 \; \ldots \; f_n) \tag{6.8}$$

is the vector of calculated quantities (range and/or range rate) which is a non-linear function of the vector x and is obtained by ray tracing the radio signal connecting the positions of ATS and NIMBUS through the assumed model (6.3) with the initial estimate of the parameters $\tilde{x}$ in (6.6). By comparing the computed values of the range or range rate f in (6.8) with the observed values z in (6.7), it is possible to correct the parameter set iteratively.

As shown in Appendix A, using a modified Newton-Raphson iteration scheme, the solution vector x* is

$$x^* = x^{(m)} + \left[B^T D_z^{-1} B + D_{\tilde{x}}^{-1}\right]^{-1} \left\{B^T D_z^{-1} \left[z - f(x^{(m)})\right] + D_{\tilde{x}}^{-1} (x - \tilde{x}^{(m)})\right\} \quad (6.9)$$

where B is an (n × m) matrix of partial derivatives (rank m < n)

$$B = \left(b_{ij} = \frac{\partial f_i}{\partial a_j}\right) = B(x) \quad (6.10)$$

and $x^{(m)}$ is the estimate of the parameter vector x at the mth iteration.

The variance of the refractivity at the normalized height s is given by

$$\sigma_N^2 = \exp(2 s^T x^*)\, s^T \left[B^T D_z^{-1} B + D_{\tilde{x}}^{-1}\right]^{-1} s \quad (6.11)$$

The standard deviation of N is the square root of (6.11).

It should be noted that the location of the specific ray connecting the two satellites is in itself an iterative procedure. Starting with a given radius of closest approach r_p (Figure 10), a ray is traced through the given atmosphere using Snell's law for a spherically stratified medium (4.4). At the assumed limit of the atmosphere (at a height of 100 kilometers for this analysis), the ray tracing is stopped and the ray asymptote is extended until it intersects the circle with radius equal to the radius vector of the satellite. The angle subtended by the two points of intersection at the center of the earth is compared with the angle subtended by the locations of ATS and NIMBUS at the center of the earth. If the

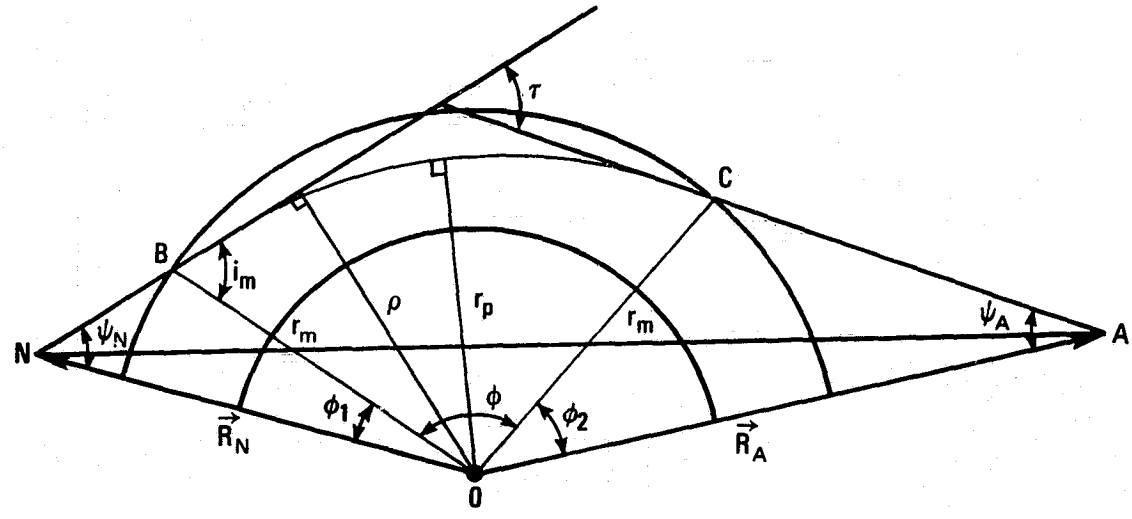

Figure 10. Occultation Geometry for Iterative Model-Fitting Technique

two angles do not agree to the required precision (10^{-9} radians), the radius of closest approach is changed and another ray is traced. A modified Newton-Raphson iterative procedure is used.

After the ray connecting the two satellites is found, the range along that ray, as well as the partial derivatives of the range with respect to the parameters of the model atmosphere are determined, (6.10) (in the case where the observations are ranges). The partial derivatives are found numerically. This procedure is repeated for all the given pairs of positions of the two satellites. Computed values of range f are compared with observed values z. If they do not agree to the required precision, the residuals along with the partial derivatives are used to estimate corrections to the parameter set x by using the least squares criterion (Appendix A). This process is repeated iteratively until the change in the parameter set is within a specified magnitude. The solution is then given by (6.9). Figure 11 gives the flowchart of the computation.

Results of Iterative Model Fitting

Simulated range data along with the sequential position and velocity coordinates of ATS and NIMBUS were used as input for the iterative model fitting technique described above. In all cases investigated the range data included both lower atmospheric and ionospheric effects. The input lower atmospheric refractivity profile was a least squares fit of N = exp [P(s)] to values of refractivity versus height calculated from radiosonde data taken at Dulles airport, Virginia, during

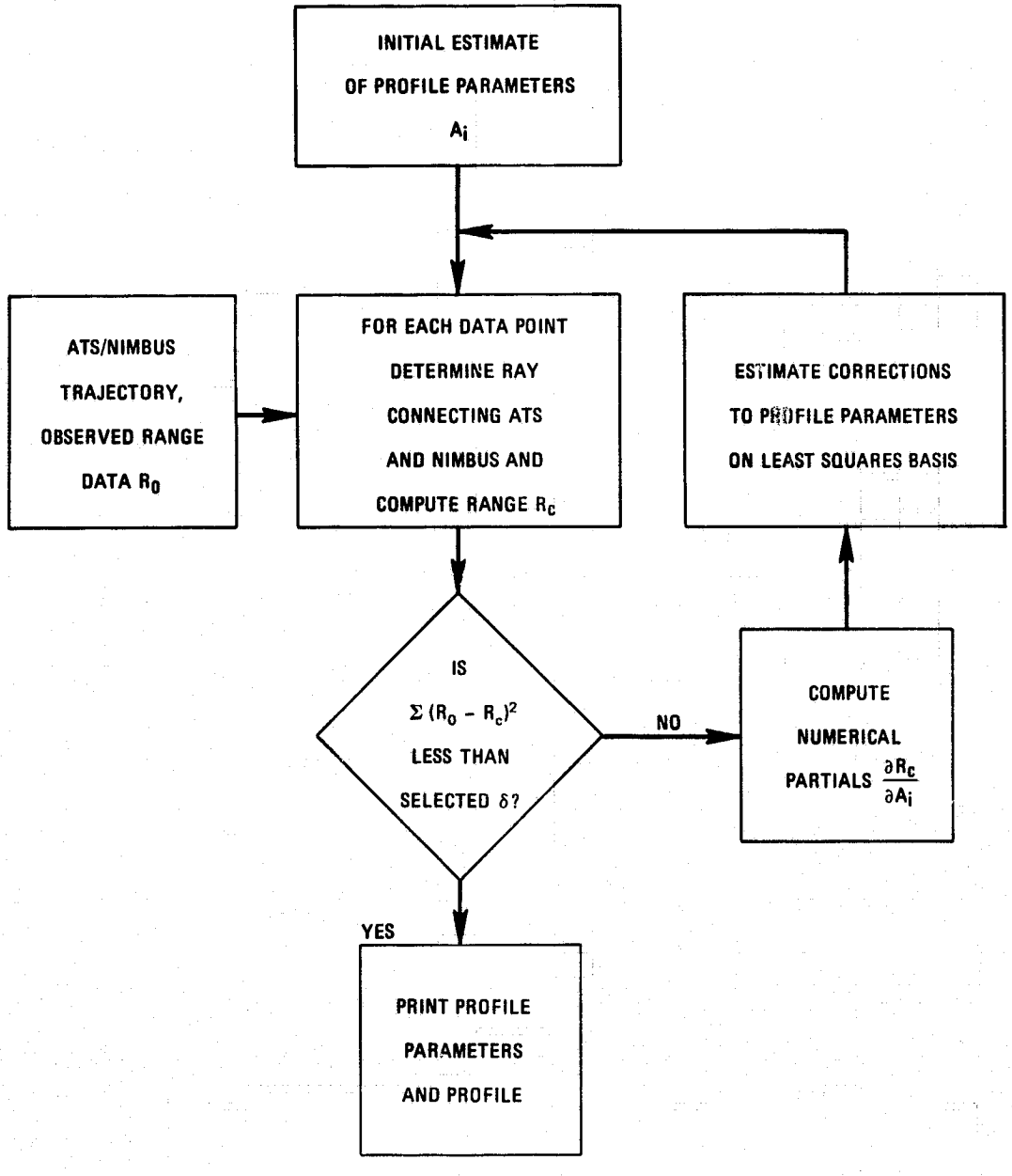

Figure 11. Flow Chart of Iterative Model-Fitting Algorithm (Range Data)

1967 where P(s) is a second degree polynomial. The input ionospheric electron density profile is a least squares fit of exp [Q(s)] to the composite profile indicated in Figure 8 where Q(s) is a seventh degree polynomial (see Table I). The results of the model fitting technique can be seen in Table II. Column 1 is the height in kilometers above the surface, Column 2 is the input lower atmospheric refractivity. In all cases the lower atmospheric refractivity profile which is "solved for" is a function of the form exp [P(s)] where P(s) is a 2nd degree polynomial.

The third column is the recovered refractivity where the input ionospheric electron density function (8 parameter model of form exp [Q(s)]) has been "modelled" into the calculations. The error in recovery is on the order of 0.05% at the surface and less than 1% at 50 kilometers.

The fourth column shows the results of neglecting the ionosphere entirely (neither "modelled" nor "solved for"). The errors in recovery are large; about 7% at the surface and about 375% at around 45 kilometers height. This clearly indicates that the ionosphere cannot be neglected at S-band frequencies.

The fifth column shows the results of modelling the Chapman function in the calculations (the parameters for this model were obtained by fitting in the least sense the Chapman function to the composite profile in Figure 8). The error in recovery is about 1.3% at the surface and 25% at 40 kilometers.

The sixth column is the recovered refractivity where the ionospheric electron density has been "solved for" and has the Chapman form. The maximum error is about 12.5% at 40 kilometers.

Finally, in the last column are shown the recovered refractivity values when the parameters of the modified Chapman function are "solved for." Recovery in this case is excellent and is seen to be approximately 0.3% at 15 kilometers (maximum).

The above demonstrates: (1) the ionosphere cannot be neglected as S-band frequencies (column 4), and; (2) a reasonably simple model for the ionospheric electron density such as the modified Chapman should be sufficiently accurate to recover lower atmospheric refractivity profiles (column 7).

7.0 THE HERGLOTZ-WIECHERT METHOD[6]

This technique was originally developed for the purpose of inverting seismic data in order to obtain velocity depth profiles of the earth. The analysis makes

Table II

Recovered Lower Atmospheric Refractivity By Iterative Model Fitting

Height (Kilometers)	Input Lower Atmospheric Refractivity	Recovered Lower Atmospheric Refractivity				
		Lower Atmospheric Refractivity Only "Solved For." Eight Parameter Ionospheric Profile "Modelled."	Lower Atmospheric Refractivity "Solved For." No Ionosphere "Modelled" or "Solved For."	Lower Atmospheric Refractivity "Solved For." Chapman Function "Modelled."	Lower Atmospheric Refractivity "Solved For." Chapman Function "Solved For."	Lower Atmospheric Refractivity "Solved For." Modified Chapman Function "Solved For."
0	375.2	375.4	348.7	370.4	372.9	375.3
5	175.3	175.3	195.8	176.2	175.9	175.3
10	81.9	81.9	110.0	83.8	83.0	81.9
15	38.3	38.3	61.8	39.9	39.1	38.2
20	17.9	17.9	34.7	18.9	18.4	17.8
25	8.3	8.3	19.5	9.0	8.7	8.3
30	3.9	3.9	10.9	4.3	4.1	3.9
35	1.8	1.8	6.1	2.0	1.9	1.8
40	0.8	0.8	3.4	1.0	0.9	0.8
45	0.4	0.4	1.9	0.5	0.4	0.4
50	0.2	0.2	0.2	0.2	0.2	0.2

Note 1: In all cases the satellite-to-satellite range data includes both lower atmospheric and ionospheric effects. The input lower atmospheric refractivity profile is a least squares fit of exp [P(s)] to values of refractivity versus height calculated from radiosonde data taken at Dulles Airport, Virginia in 1967 where P(s) is a second degree polynomial. The input ionospheric electron density profile is a least squares fit of exp [Q(s)] to the composite profile in Figure 8 (Q(s) is a 7th degree polynomial, see Table I).

Note 2: In all cases above the lower atmospheric refractivity profile which is "solved for" (in the least squares sense) is a 3 parameter model of the form $N = \exp [P(s)]$.

Note 3: In the above the term "modelled" (e.g. Chapman function "modelled") means the least squares fit of that function to the composite profile (indicated in Figure 8 and Table I) was fixed in the calculations.

use of the Abel transform for the integral describing the phase change along a bent ray path. This method has been adapted for radio occultation data by Phinney and Anderson [20] whose derivation is given in Appendix C. The refractivity index n, corresponding to a radius r is given by

$$n(r) = \exp\left[(1/\pi)\int_{r_m}^{\eta} \cosh^{-1}(\rho/\eta)\left(\frac{1}{\rho}\right)\frac{dP_a}{d\rho}\,d\rho\right] \qquad (7.1)$$

where $P_a = P(\rho) - 2r_m \cos i_m$, i_m is the angle of incidence at the outer limit of the atmosphere, and $P(\rho)$ is the phase path length (equation C.2). See Figure 12.

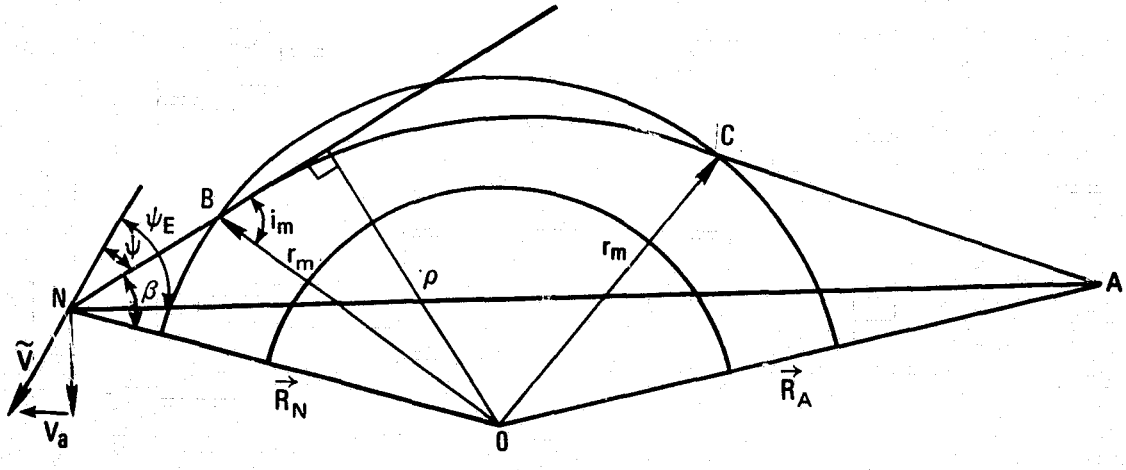

Figure 12. Occultation Geometry for Herglotz-Wiechert Technique

[6]This section is self-contained. The notation used is different from that used elsewhere in the report.

Computation of Impact Parameter

It can be shown [20] that the angle between the satellite (NIMBUS) trajectory and the ray path ψ (Figure 12) is given by

$$\cos \psi = (D_e + D_a)/\tilde{V} \tag{7.2}$$

where D_e is the contribution to the rate of phase path change due to the motion of the satellite and D_a the contribution due to the atmospheric refraction effect. $\tilde{V}$ is the projection of the velocity of NIMBUS on the plane containing NIMBUS, ATS, and the center of the earth. Similarly, the angle between the trajectory of NIMBUS and the line of sight between the two satellites is given by

$$\cos \psi_e = D_e/\tilde{V} \tag{7.3}$$

The range rate between the two satellites can be shown to be the sum of the projection of the velocity vector of each satellite along the ray path.

When there is no atmosphere the true range rate $\dot{R}_T$ is given by

$$\dot{R}_T = V_{NL} + V_{AL} \tag{7.4}$$

where V_{NL} is the projection of the velocity vector of NIMBUS along the line of sight and V_{AL} is the projection of the velocity vector of ATS along the line of sight. From (7.3)

$$\cos \psi_e = V_{NL}/\tilde{V} \tag{7.5}$$

Combining (7.4) and (7.5) we get

$$\psi_e = \cos^{-1} \left[(\dot{R}_T - V_{AL})/\tilde{V}\right] \tag{7.6}$$

Similarly we can show

$$\psi = \cos^{-1}\left[(\dot{R} - V_{AR})/\tilde{V}\right] \tag{7.7}$$

where $\dot{R}$ is the measured range rate through the atmosphere and V_{AR} is the projection of the velocity vector of ATS along the ray path.

From Figure 12 we see that the impact parameter ρ is given by

$$\rho = |\vec{R}_N| \sin\beta \tag{7.8}$$

where $|\vec{R}_N|$ is the radial distance of NIMBUS and

$$\beta = \psi_e - \psi + <ONA \tag{7.9}$$

Hence, by knowing ψ, ψ_e, and the trajectories of NIMBUS and ATS it is possible to compute the impact parameter.

However, the computation of ψ requires a knowledge of the ray path (equation 7.7). But to start with, the ray path which is uniquely defined by the impact parameter, is not known. Hence it is necessary to undertake an iterative procedure to determine the impact parameter.

As a first approximation it is assumed that $V_{AR} = V_{AL}$, and ψ, ψ_e and ρ are computed. Now

$$\sin i_m = \rho / r_m \tag{7.10}$$

By knowing i_m it is possible to compute the direction cosines of the ray at ATS and hence V_{AR} The new value of V_{AR} is then input to determine a new value of ρ. This process is continued until convergence is reached.

Computation of Refractivity

The evaluation of refractivity from equation (7.1) is done in the following steps:

(1) The input data consisting of position and velocity of the two satellites as a function of time, the range and range rate along the propagation path, are read in.

(2) For each data point the impact parameter is computed as described in the above. The range residual P_a (equation 7.1) is also computed for each data point by subtracting the linear segments of the ray from the top of the atmosphere to each satellite from the range. In addition the term $2 r_m \cos i_m$ is also subtracted from the range.

(3) The logarithm of P_a is then fitted as a polynomial in ρ, normalized between the limits -1 and +1. It is then possible to obtain $(dP_a / d\rho)$ analytically from the polynomial coefficients.

(4) Finally, the refractive index $n(r)$ is obtained from equation (7.1) by numerical quadrature. Gaussian quadrature with 32 intervals is used after subdividing the range of integration into a number of subintervals.

An example of a recovered lower atmospheric refractivity profile using the Herglotz-Wiechert algorithm is shown in Table III. The input profile is the same as that assumed for the first example in the iterative technique (Section 6.0). Recovery is .4% accurate at the surface and 40% accurate at 33 kilometers.

Table III
Results of Inversion by H-W Algorithm
for the Three Parameter Profile

Radius (km)	Refractivity Computed from the H-W Algorithm	Refractivity from the Input Profile	Difference
6379.02	320.2	321.4	1.2
6381.71	212.2	213.5	1.3
6384.13	146.3	147.7	1.4
6386.40	103.1	104.5	1.4
6388.59	73.4	74.9	1.5
6390.72	52.7	54.1	1.4
6392.82	37.9	39.3	1.4
6394.88	27.3	28.7	1.4
6396.93	19.7	21.0	1.3
6398.97	14.1	15.4	1.3
6401.00	10.1	11.3	1.2
6403.01	7.1	8.3	1.2
6405.03	5.0	6.1	1.1
6407.04	3.4	4.5	1.4
6409.05	2.3	3.3	1.0
6411.05	1.5	2.4	.9

8.0 RECOVERY OF PRESSURE AND TEMPERATURE

Refractivity at radio frequencies has been previously defined (equation 3.1) as

$$N = 77.6\,(P/T) + (3.73)10^5\,(e/T^2) \tag{8.1}$$

If the wet component of N (second term on right side of (8.1)) can be properly modelled or determined (e.g. by an independent measurement), the remaining part, N_{dry}, is proportional to density, a function of both pressure and temperature

$$N_{dry} = 77.6\,(P/T) \tag{8.2}$$

Assuming hydrostatic equilibrium and the perfect gas law, the pressure at a given height can be obtained by integrating N_{dry} [21]. The temperature at the given height can then be calculated from (8.2).

The hydrostatic equation is [13]

$$dP = -\rho\, g(z)\, dz \tag{8.3}$$

where g(z) is ([22], pg. 217)

$$g(z) = g_0\, r_0^2/(r_0 + z)^2 \qquad (m/sec^2) \tag{8.4}$$

and g_0, the local acceleration of gravity is calculated from the latitude ϕ_L ([22], pg. 488)

$$g_0 = 9.780356\,(1 + 0.0052885\,\sin^2\phi_L - 5.9\times10^{-6}\,\sin^2 2\phi_L) \tag{8.5}$$

The effective earth's radius r_0 in (8.4) is given by ([22], pg. 218)

$$r_0 = 2g_0/f(\phi_L) \tag{8.6}$$

where

$$f(\phi_L) = 3.085462 \times 10^{-6} + 2.27 \times 10^{-9} \cos 2\phi_L - 2 \times 10^{-12} \cos 4\phi_L \quad (8.7)$$

In the above equations z is the geometric height and dz is the differential geometric height, both in geometric kilometers.

The perfect gas law is ([13])

$$\rho = MP/RT_v \quad (8.8)$$

where

M = the apparent molecular weight of dry air = 28.966 ([22], pg. 289)

R = universal gas constant = 8314.36 Joules $(°K)^{-1} \times (Kg\text{-}mole)^{-1}$ ([22], pg. 289)

P = pressure in millibars

T_v = virtual temperature in degrees Kelvin

ρ = density of dry air

Substituting (8.8) in (8.3) and using (8.2)

$$dP = \left(\frac{-Mg(z)}{77.6\,R}\right) (T/T_v)\, N_{dry}\, dz \quad (8.9)$$

Taking the integral of both sides of (8.8), the pressure P at the height h is obtained

$$P = \frac{M}{77.6\,R} \int_h^\infty g(z)\, (T/T_v)\, N_{dry}\, dz$$

or

$$P = (M/77.6\,R) \int_h^\infty g(z)\,(T/T_v)\,(N - N_w)\,dz \tag{8.10}$$

The temperature T can be obtained using (8.2) and (8.10).

From (8.10) it can be seen that, having recovered the total refractivity N, the wet component, N_{wet}, must be subtracted out. In addition (T/T_v) must be modelled.

Using tables of the U.S. Standard Atmosphere Supplements [13] a regression model for both (T/T_v) and N_w was obtained from 9 Standard atmospheres.

For 15° North Annual and the 4 January atmospheres (30°N, 45°N, 60°N, 75°N), the following regression models were obtained

$$\ln \ln (T_v/T) = (-3.0557 - 0.0648\,\phi_L) + [-0.6192 + 0.0043\,\phi_L]\,h$$

$$\ln \hat{N}_w = (5.678 - 0.0488\,\phi_L) + [-0.5897 + (0.1104)\,10^{-2}\,\phi_L]\,h \tag{8.11}$$

where ϕ_L is the latitude in degrees and h the altitude in kilometers.

For the July atmospheres (30°N, 45°N, 60°N, 75°N), the following regression models were obtained

$$\ln \ln (T_v/T) = (-3.7414 - 0.0234\,\phi_L) - 0.4389\,h$$

$$\ln \hat{N}_w = 5.4510 - 0.0186\,\phi_L - 0.4529\,h - (0.1756)\,10^{-2}\,\phi_L\,h \tag{8.12}$$

Equation (8.10) can be written as

$$P_c = \int_h^{h_T} K(\phi_L, z)\,\hat{N}_d(z)\,dz \tag{8.13}$$

where

$$K(\phi_L, z) = \left(\frac{M}{77.6\,R}\right)\left(\frac{T}{T_v}\right) g(z)$$

$$\hat{N}_d = N - \hat{N}_w$$

and (T/T_v) and $\hat{N}_w$ are given by either (8.11) or (8.12).

Example

From radiosonde data taken at Dulles airport in January 1967, the dry, wet, and total refractivity, $N = N_d + N_w$ were calculated from measured values of temperature, pressure and relative humidity using (3.1) and the procedure documented in [15]. Both (T/T_v) and $\hat{N}_w$ were estimated from (8.11) and the integrand in (8.10) numerically integrated from the height h to 200 kilometers to obtain P_c. T_c was obtained from (8.2). The results can be seen in Table IV. Recovery of pleasure is accurate to within 0.3%. The temperature recovery is worst at the surface, but improves with height.

Table IV

Pressure and Temperature Recovery From Estimated Dry Refractivity

Height (km)	Dry Refractivity $\hat{N}_d = N - \hat{N}_w$	Pressure P (mb)	Calculated Pressure $P_c = \int_h^{h_T} K(\phi_L, h)\, \hat{N}_d\, dh$	$100\left(\frac{P_c - P}{P}\right)$	T (°K)	$T_c = \frac{77.6\, P_c}{\hat{N}_d}$	$\frac{100\,(T_c - T)}{T}$
0	270.67	1005	1002.16	-0.29	273.15	287.32	5.19
1	254.53	886.47	885.95	-0.06	271.81	270.10	-0.63
2	222.41	787.69	788.68	0.13	271.70	275.18	1.28
3	199.19	695.32	696.84	0.22	271.25	271.48	0.08
4	180.14	609.28	610.36	0.18	264.47	262.93	-0.58
5	163.19	538.04	538.51	0.09	257.79	256.08	-0.66
10	91.20	265.45	265.45	0.07	225.41	225.86	0.20
20	19.94	54.47	54.47	0.27	211.54	211.55	0.27

9.0 SUMMARY

Two techniques for recovering lower atmospheric refractivity profiles from simulated satellite-to-satellite tracking data have been described and examples given using the geometric configuration of the ATS-6/NIMBUS-6 Tracking Experiment. Both satellites are in circular orbit (NIMBUS in polar orbit and ATS in geostationary orbit in equatorial plane) and the underlying atmospheric refractivity has the symmetric form $N = \exp P(s)$ where $P(s)$ is a polynomial in the normalized height s. For purposes of recovery, a second degree polynomial was used for $P(s)$.

For the particular simulation used in the analysis, the Herglotz-Wiechert technique recovered values which were 0.4% and 40% different from the input values (calculated from the parameters of the assumed model atmosphere) at the surface and at a height of 33 kilometers respectively. Using the same input data, the model fitting technique recovered refractivity values 0.05% and 1% different from the input values at the surface and at a height of 50 kilometers, respectively.

It should be noted that modelling errors have not been included in the above. The examples cited show the relative degradation in the accuracy due to the calculation method rather than the true accuracy.

The possible application of recovering atmospheric refractivity profiles lies in the area of meteorology. If the effects of the ionosphere and water vapor can be properly modelled or removed from the data, then calculation of pressure and temperature distributions can be made from the dry refractivity through numerical integration procedures. This has been demonstrated using radiosonde data from Dulles airport, Virginia, calculating the total refractivity from measured values of temperature, pressure, and relative humidity, and using a regression model (obtained from 9 Standard atmospheres) to subtract out the wet refractivity. The term (T/T_v) in the integrand of (8.10) was estimated from a regressional model (also obtained from 9 Standard atmospheres) and finally equation (8.10) numerically integrated from a height h to 200 kilometers to obtain pressure. The temperature was then obtained from (8.2). Pressure recovery was less than 0.3% to 20 kilometers. Temperature recovery at the surface was 5% but improved with height.

The techniques documented here will be applied to the calculation of lower atmospheric refractivity profiles from actual satellite-to-satellite tracking data taken during the radio occultation portion of the ATS-6/NIMBUS-6 Tracking and Orbit Determination Experiment. The basic approach will be the iterative model fitting technique, using the Herglotz-Wiechert technique as a "starter" to obtain an initial estimate of the parameter vector (apriori values). It is planned to obtain radiosonde data as close as possible to the point where the ray path of the

signal between the two satellites comes closest to the earth at the time of occultation. From the radiosonde data refractivity profiles will be calculated to verify and compare against those obtained by radio occultation methods. In addition both pressure and temperature distributions will be obtained using the procedure described above and compared against the radiosonde data.

Along with the analysis of the occultation data from ATS/NIMBUS there will be a continuing effort to model the water vapor and investigate horizontal gradients using regression techniques.

10. CONCLUSIONS

(1) Two techniques for recovering lower atmospheric refractivity profiles from simulated satellite-to-satellite tracking data have been documented — the Herglotz-Wiechert algorithm employing the integral Abel transform and an iterative model fitting method incorporating a numerical ray tracing procedure. Of the two the model fitting technique recovered the input profile more accurately.

(2) For accurate inversion of lower atmospheric refractivity profiles, it is necessary to take the ionospheric refraction of the ray into account. A simple model of the ionospheric electron density like the modified Chapman profile has been shown to be adequate for accurate recovery of the lower atmospheric profile.

(3) By properly modelling the ionosphere and water vapor effects (through regression techniques), it is possible to obtain pressure and temperature distributions from the dry refractivity using the hydrostatic equation and the perfect gas law.

REFERENCES

1. Schmid, P. E., and Vonbun, F. O., "The ATS-F/NIMBUS-F Tracking and Orbit Determination Experiment," NASA, Goddard Space Flight Center, Greenbelt, Md., 1973.

2. Colin, L., "Mathematics of Profile Inversion," Proc. of Workshop Held at Ames Research Center, NASA TM X-62, 150., August 1972.

3. Kliore, Arvydas; Cain, L.; Levy, Gerald S.; Eshleman, Von R.; Fjeldbo, Gunnar; and Drake, Frank D., "Occultation Experiment: Results of the First Direct Measurement of Mars Atmosphere and Ionosphere," Science, Vol. 149, No. 3689, Sept. 1965, pp. 1243-1248.

4. Fjeldbo, Gunnar; Fjeldbo, Wencke C.; and Eshleman, Von R, "Models for the Atmosphere of Mars Based on Mariner 4 Occultation Experiment," J. Geophys. Res., Vol. 71, no. 9, May 1966, pp. 2307-2316.

5. Fjeldbo, Gunnar; and Eshleman, Von R., "The Atmosphere of Mars Analyzed by Integral Inversion of the Mariner IV Occultation Data," Planet. Space Sci., Vol. 16, no. 8, Aug. 1968, pp. 1035-1059.

6. Kliore, Arvydas; Levy, Gerald S.; Cain, Dan L.; Fjeldbo, Gunnar; and Rasool, S. I., "Atmosphere and Ionosphere of Venus From the Mariner V S-Band Radio Occultation Measurement," Science, Vol. 158, no. 3809, Dec. 1967, pp. 1683-1688.

7. Mariner Stanford Group: "Venus: Ionosphere and Atmosphere as Measured by Dual-Frequency Radio Occultation of Mariner V," Science, Vol. 158, no. 3809, Dec. 1967, pp. 1678-1683.

8. Fjeldbo, G.; and Eshleman, V. R., "Atmosphere of Venus as Studied With The Mariner V Dual Radio Frequency Occultation Experiment," Radio Science, Vol. 4, no. 10, Oct. 1969, pp. 879-897.

9. Marini, J. W., Memorandum to Dr. F. O. Vonbun, "ATS-NIMBUS Occultation Experiment," December 13, 1972.

10. Bryan, G. W., Lynn, J. J., Hinely, A. O., "A User's Guide For Satellite-To-Satellite System Observations And Data Formats," GSFC (NASA), X-932-75-78, March 1975.

11. Bean, B. and Dutton, E., "Radio Meteorology," NBS Monograph 92, March 1, 1966.

12. Berry, F., Bollay, E., and Beers, N., "Handbook of Meteorology," McGraw Hill, N.Y., 1945.

13. U.S. Standard Atmosphere Supplements, 1966, ESSA, NASA, USAF.

14. Bean, B., and Thayer, G. D., "CRPL Exponential Reference Atmosphere," National Bureau of Standards, Monograph 4, Oct. 1959.

15. Marini, J. W., and Murray, Jr., C. W., "Correction of Laser Range Tracking Data For Atmospheric Refraction at Elevations Above 10 Degrees," GSFC (NASA), X-591-73-351, November 1973.

16. Bean, B. R., Thayer, G. D., "Models of the Atmospheric Radio Refractive Index," Proc. of the IRE Vol. 47, May 1959, pp. 740-755.

17. Schmid, P. E., "Atmospheric Tracking Errors at S and C-Band Frequencies," NASA TND-3470, August 1966.

18. Chandra, S., "Electron Density Distribution in the Upper F Region," Journal of Geophysical Research, Vol. 68, pp. 1937-1942, 1963.

19. Rangaswamy, S., and Jackson, J. E., "Intercomparison of Electron Content Obtained From Farady Rotation and From Combined Satellite and Ground-Based Soundings," Paper presented at the 1972 American Geophysical Union Conference at San Francisco, Fall 1972.

20. Phinney, R. A., Anderson, D. L., "On the Radio Occultation Method for Studying Planetary Atmospheres," Journal of Geophysical Research, Vol. 73, No. 5, March 1, 1968, pp. 1819-1827.

21. Marini, J. W., Private Communication.

22. List, R. J., "Smithsonian Meteorological Tables," Sixth Revised Edition (Second Reprint), Publication 4014, 1963.

APPENDIX A

WEIGHTED NONLINEAR LEAST SQUARES WITH APRIORI PARAMETER VECTOR AND COVARIANCE MATRIX[1]

The particular numerical method used to solve the nonlinear least squares problem is a modified Newton-Raphson iteration technique.

Let $\mathbf{z}$ be an $(n \times 1)$ vector of measurements and $f(x)$ a nonlinear function or model which it is assumed adequately describes the measurements, where x is an $(m \times 1)$ parameter vector.

$$\mathbf{z} = (z_1, z_2, \ldots, z_n)$$
$$\mathbf{x} = (x_1, x_2, \ldots, x_m) \qquad \text{(A.1)}$$

It should be noted that in the occultation problem where the refractivity has the form $N = \exp P(s)$ and $P(s) = a_0 + a_1 s + a_2 s^2 + \ldots + a_{m-1} s^{m-1}$ is a polynomial in the normalized height $s = (.01)h - 1$ (h is height in kilometers), x is the $(m \times 1)$ parameter vector of coefficients a_j. The vector $\mathbf{z}$ is the vector of observed ranges between the two satellites or the vector of observed range rates along the propagation path of the signal, or both of these quantities. The function $f(x)$ is a function of the parameter vector x which can be the calculated range, range rate, or both. In any case, the parameters a_j enter in a nonlinear fashion in the calculation of these quantities (ray tracing of angles and distances within the troposphere). We can write

$$f^T = (f_1, f_2, \ldots, f_n) \qquad \text{(A.2)}$$

where f_i represents the value of range (or range rate) calculated for the ith data point for a particular set of values for x (i.e., the a_i's).

[1]This appendix is self contained. The notation is therefore general.

PRECEDING PAGE BLANK NOT FILMED

Let $\tilde{x}$ be an apriori estimate of the parameter vector x with its associated covariance matrix $D_{\tilde{x}}$ ($m \times m$ matrix). Let D_z be the covariance matrix of the observation vector z. The function that we wish to minimize is the quadratic form

$$Q = \left[z - f(x)\right]^T D_z^{-1} \left[z - f(x)\right] + (x - \tilde{x})^T D_{\tilde{x}}^{-1} (x - \tilde{x}) \qquad (A.3)$$

where

$$\tilde{x}^T = (\tilde{x}_1, \tilde{x}_2, \ldots, \tilde{x}_m) \qquad (A.4)$$

In a statistical sense we can consider the apriori values as random variables (or additional observations) having the mean vector x. The covariance matrix $D_{\tilde{x}}$ then represents the confidence or certainty that we have in our "best" estimate $\hat{x}$ of the parameter vector x. As an example of how one might arrive at values for $\tilde{x}$ and $D_{\tilde{x}}$, suppose that from tabular values of pressure, temperature, and relative humidity (either radiosonde data from a particular weather station or data from a standard atmosphere) a refractivity profile is calculated as a function of height. Using linear least squares we can then fit the logarithm of the calculated values of refractivity with a polynomial of degree (m - 1). The solution vector of coefficients a_j and its covariance matrix could then be used as an apriori parameter vector $\tilde{x}$ with covariance matrix $D_{\tilde{x}}$ for a subsequent occultation problem. In another sense the matrix $D_{\tilde{x}}$ serves as a control in the iteration process. From (A.3) it can be seen that if $D_{\tilde{x}}$ is very large (large uncertainty in $\tilde{x}$), then $D_{\tilde{x}}^{-1}$ will be very small and the second term on the right side of (A.3) becomes negligible, which means that the observations "take over" and determine the solution (standard least squares problem); if the opposite is true, i.e., $D_{\tilde{x}}$ is very small, the solution will be near the apriori vector $\tilde{x}$. Thus, $D_{\tilde{x}}^{-1}$ serves as a weighting matrix for the apriori values. In a similar manner we can talk about the matrix D_z which is usually taken as diagonal (observations are uncorrelated). For least squares with equal weighting D_z is a scalar times the identity matrix I.

In order for (A.3) to be minimized, it is necessary that the gradient of Q with respect to x, $\nabla_x Q$, evaluated at the solution $x = x^*$, vanish

$$F(x) = \nabla_x Q = -2 B^T D_z^{-1} \left[z - f(x)\right] - 2 D_x^{-1} (\tilde{x} - x) \qquad (A.5)$$

where

$$B = \left(b_{ij} = \frac{\partial f_i}{\partial x_j} \right) = B(x) \qquad \text{(A.6)}$$

is an $(n \times m)$ matrix of partial derivatives of the calculated quantities with respect to the parameters of rank $m < n$.

Neglecting the dependence of B on x a modified Newton-Raphson iteration technique can be used to find a solution x^* such that $F(x^*) = 0$. Taking the gradient of $F(x)$ with respect to x

$$F'(x) = \nabla_x^2 Q = 2 B^T D_z^{-1} B + 2 D_{\tilde{x}}^{-1} \qquad \text{(A.7)}$$

Since both D_z and D_x are covariance matrices, they are by definition positive definite. Since B is assumed to be of rank $m < n$, $B^T D_z^{-1} B$ is positive definite. Therefore (A.7) is positive definite, and if the process converges to x^*, Q will be minimized.

In order to solve for x^*, denote by $x^{(m)}$ the estimate of the solution at the mth iteration; then, the improved estimate of the solution $x^{(m+1)} = x^*$, using the Newton-Raphson formula will be given by

$$x^* = x^{(m+1)} = x^{(m)} - F(x^{(m)}) / F'(x^{(m)})$$

or

$$x^* = x^{(m)} + (B^T D_z^{-1} B + D_{\tilde{x}}^{-1})^{-1} \left\{ B^T D_z^{-1} \left[z - f(x^{(m)}) \right] + D_{\tilde{x}}^{-1} (\tilde{x} - x^{(m)}) \right\} \qquad \text{(A.8)}$$

where

$$B = B(x^{(m)})$$

Assuming the observations z to be independent (in the statistical sense) of the apriori values $\tilde{x}$, the covariance matrix of the solution x^* is given by

$$D_{x^*} = (B^T D_z^{-1} B + D_{\tilde{x}}^{-1})^{-1} \tag{A.9}$$

The Uncertainty in Refractivity

Let the refractivity model be given by

$$N = \exp s^T x^* = \exp P(s) \tag{A.10}$$

where x^* is the solution vector

$$(x^*)^T = (a_0^*, a_1^*, \ldots, a_{m-1}^*)$$

and

$$s^T = (1 \; s \; \ldots \; s^{m-1}) \tag{A.11}$$

is an $(m \times 1)$ vector of normalized heights $s = (0.01)h - 1$ (h is height in kilometers).

An error ΔN in the neighborhood of the solution x^* is

$$\begin{aligned} \Delta N &= \exp\left[s^T (x^* + \Delta x)\right] - \exp (s^T x^*) \\ &\doteq \left[\exp (s^T x^*)\right] s^T \Delta x \end{aligned} \tag{A.12}$$

The variance of ΔN (or of N) is, using (A.9)

$$\sigma_{\Delta N}^2 = \exp (2 s^T x^*) \, s^T \left[B^T D_z^{-1} + D_{\tilde{x}}^{-1}\right]^{-1} s \tag{A.13}$$

The uncertainty or standard deviation of N is the square root of (A.13).

APPENDIX B

RAY TRACING THROUGH THE LOWER ATMOSPHERE AND IONOSPHERE

From Fermat's principle of extremal path and the Euler-Lagrange variational equation, we obtain for a ray,

$$n(r) \cdot r \sin i = \rho \tag{B.1}$$

where n is the phase refractive index, r the geocentric radius, i the angle of incidence and ρ the distance of the ray asymptote from the earth's center. The total bending angle τ (Figure 10) is given by

$$\tau = -2 \int_{r_p}^{r_m} \frac{1}{n(r)} \frac{dn(r)}{dr} \frac{dr}{\sqrt{\eta^2 - \rho^2}} \tag{B.2}$$

where $\eta = n(r) \cdot r$

r_p = radius of closest approach of the ray

r_m = radius of the outer limit of the atmosphere

The angle subtended by the total arc of the ray in the atmosphere at the center of the earth ϕ is given by

$$\phi = \tau + \pi - 2i_m \tag{B.3}$$

where i_m is the angle of incidence at the outer limit of the atmosphere given by

$$i_m = \sin^{-1}\left(\frac{\rho}{r_m}\right) \tag{B.4}$$

The computed value of the angle subtended by the total ray path at the center of the earth is given by

$$\theta_c = \phi_1 + \phi_2 + \phi \tag{B.5}$$

where ϕ_1 and ϕ_2 are the angles subtended at the center of the earth by the linear segments of the ray.

The observed angle subtended by the total ray path at the center of the earth is given by

$$\theta_0 = \cos^{-1} \frac{\vec{R}_n \cdot \vec{R}_A}{\vec{R}_N \quad \vec{R}_A} \tag{B.6}$$

where $\vec{R}_N$ and $\vec{R}_A$ are the radius vectors of NIMBUS and ATS respectively. The ray linking NIMBUS and ATS for a given atmosphere is found by iteratively altering r_p until θ_c agrees with θ_0 to within the required precision.

After finding the specific ray linking ATS and NIMBUS, the one-way range along that ray is computed from

$$R_c = NB + CA + P \tag{B.7}$$

where NB and CA are the linear segments of the ray which can be calculated from a knowledge of $\vec{R}_N$, $\vec{R}_A$, r_m, and i_m. P is the path length of the ray in the atmosphere.

The lower atmosphere is non-dispersive for radio waves and hence P is given by

$$P_T = 2 \int_{r_p}^{r_m} \frac{n(r)}{\cos i} \, dr \tag{B.8}$$

$$= 2 \int_{r_p}^{r_m} \frac{\eta^2 \, dr}{r \sqrt{\eta^2 - \rho^2}}$$

The ionosphere is dispersive and here P is given by

$$P_I = 2 \int_{r_p}^{r_I} \frac{n_g(r)\, dr}{\cos i} \tag{B.9}$$

where n_g is the group refractive index.

$$n_g = \frac{d}{df}(nf) \tag{B.10}$$

and f is the frequency of transmission, n is the phase index of refraction. At S-band frequencies (2 MHz), P can be written as

$$P_I = 2 \int_{r_p}^{r_I} \frac{r\, dr}{\sqrt{\eta^2 - \rho^2}} \tag{B.11}$$

where r_I is the radius of the upper limit of the ionosphere (altitude of 1000 kilometers for this analysis).

The integrals (B.2), (B.9), and (B.11) are evaluated by Gaussian quadrature.

The range rate between the two satellites is obtained by the algebraic addition of the component of the velocity of each satellite along the ray path at the satellite. The ray path direction at each satellite is found by knowing the angle between the ray path and the radial line from the center of the earth to the satellite. For NIMBUS (Figure 10) this angle ψ_N is

$$\psi_N = \sin^{-1}\left(\frac{\rho}{\vec{R}_N}\right) \tag{B.12}$$

Similarly, the angle between the ray path and the radius at ATS ψ_A is given by

$$\psi_A = \sin^{-1}\left(\frac{\rho}{|\vec{R}_A|}\right) \tag{B.13}$$

APPENDIX C

HERGLOTZ-WIECHERT ALGORITHM FOR INVERSION OF PHASE DATA

From Fermat's principle of extremal path and the Euler-Lagrange variational equation we obtain for a ray

$$n(r) \cdot r \sin i = \rho \tag{C.1}$$

where ρ is the distance of the ray asymptote from the earth's center, n is the phase index of refraction at a radial distance r and i is the angle of incidence.

The phase path length P along the ray is given by

$$P(\rho) = 2 \int_{\rho}^{r_m} \frac{\eta^2}{r \sqrt{\eta^2 - \rho^2}} \left(\frac{dr}{d\eta}\right) d\eta \tag{C.2}$$

where $\eta = n(r) \cdot r$

and r_m is the radius to the outer limit of the atmosphere.

Transforming variables

$$y = r_m^2 - \eta^2$$

$$w = r_m^2 - \rho^2$$

we obtain

$$P(w) = -2 \int_0^w \frac{(r_m^2 - y) \left[d(\ln r)/dy\right]}{\sqrt{w - y}} \, dy \tag{C.3}$$

The Abel transform of P(w) is

$$g'(y) = (r_m^2 - y) \frac{d(\ln r)}{dy} \tag{C.4}$$

or

$$g'(y) = \frac{d}{dy}\left[- \frac{1}{2\pi} \int_0^y \frac{f(w)}{\sqrt{y - w}} \cdot dw \right] \tag{C.5}$$

Transforming back from y and w to η and ρ respectively

$$\frac{d(\ln r)}{d\eta} = \left(\frac{1}{\eta^2}\right) \frac{d}{d\eta} \left[\frac{1}{\pi} \int_{r_m}^{\eta} \frac{\rho P(\rho)\, d\rho}{\sqrt{\rho^2 - \eta^2}} \right] \tag{C.6}$$

By integrating (C.6), changing the order of integration and by successive integration by parts we obtain

$$r(\eta) = r_m \exp \left[- \frac{1}{\pi} \int_{r_m}^{\eta} \cosh^{-1} (\rho/\eta)\ (1/\rho)\ \frac{dP\, d\rho}{d\rho} \right] \tag{C.7}$$

$$n(r) = \eta / r(\eta) \tag{C.8}$$

At the turning point of the ray

$$\sin i = 1$$

$$\eta_p = n_p r_p = \rho = r_m \sin i_m' \tag{C.9}$$

where the subscript p refers to the turning point.

By combining (C.7), (C.8), and (C.9) we get

$$n_p = \sin i_m \exp\left[(1/\pi) \int_{r_m}^{\eta} \cosh^{-1}(\rho/\eta) \frac{1}{\rho} \frac{dP\, d\rho}{d\rho}\right] \tag{C.10}$$

By considering the total phase change as the sum of the phase change P_e due to the relative motion of the satellites in vacuum and the phase change P_a due to the atmosphere we can write

$$P(\rho) = P_e + P_a \tag{C.11}$$

Hence, in the absence of an atmosphere

$$P(\rho) = P_e$$

and

$$1 = \sin i_m \exp\left[(1/\pi) \int_{r_m}^{\eta} \cosh^{-1}(\rho/\eta) \frac{1}{\rho} \frac{dP_e\, d\rho}{d\rho}\right] \tag{C.12}$$

Hence, we can rewrite (C.10) as

$$n_p = \exp\left[(1/\pi) \int_{r_m}^{\eta} \cosh^{-1}(\rho/\eta) \frac{1}{\rho} \frac{dP_a\, d\rho}{d\rho}\right] \tag{C.13}$$